Am J Physiol Heart Circ Physiol 283: H2660–H2670, 2002.
First published August 22, 2002; 10.1152/ajpheart.00003.2002.

Free nitric oxide diffusion in the bronchial microcirculation

PETER CONDORELLI[1] AND STEVEN C. GEORGE[1,2]
[1]*Department of Chemical Engineering and Materials Science and* [2]*Department of Biomedical Engineering, University of California, Irvine, California 92697-2575*

Received 3 January 2002; accepted in final form 12 August 2002

Condorelli, Peter, and Steven C. George. Free nitric oxide diffusion in the bronchial microcirculation. *Am J Physiol Heart Circ Physiol* 283: H2660–H2670, 2002. First published August 22, 2002; 10.1152/ajpheart.00003.2002.—Theoretical mass transfer rates and concentration distributions were determined for transient diffusion of free nitric oxide (NO) generated in vivo from vascular endothelial cells. Our analytical framework is typical of the bronchial circulation in the human pulmonary system but is applicable to the microvascular circulation in general. We characterized mass transfer rates in terms of the fractional mass flux across a boundary relative to the total endothelial NO production rate. NO concentration in the tissue surrounding blood vessels was expressed in terms of fractional soluble guanylate cyclase (sGC) activity. Our results suggest that endothelium-derived free NO is capable of vascular smooth muscle dilation despite its rapid consumption by hemoglobin in blood. An optimal blood vessel radius of 20 μm was estimated for NO signaling. We hypothesize intermittent generation of endothelial NO as a possible mechanism for sGC activation in vascular smooth muscle. This mechanism enhances the efficacy of NO-modulated vascular smooth muscle dilation while minimizing NO losses to blood and surrounding tissue.

diffusion; mass transfer; endothelium; smooth muscle dilation

ENDOTHELIUM-DERIVED relaxing factor (EDRF), a vasodilator released by arterial endothelial cells, has been identified as either free nitric oxide (NO) or a closely related compound (19). The role of NO as a ubiquitous intercellular messenger is well documented (1, 10, 52). NO is generated in vivo by the enzymatic conversion of L-arginine (L-Arg) to L-citrulline, which is catalyzed by nitric oxide synthase (NOS). The constitutive membrane-bound isoform, endothelial NOS (eNOS), produces NO in vascular endothelial cells, resulting in the dilation of blood vessels. NO activates the soluble isoform of the allosteric enzyme guanylate cyclase (sGC), which catalyzes the conversion of guanosine 5′-triphosphate to cGMP. The subsequent rise in cGMP concentration ultimately results in the dilation of smooth muscle. sGC activity is partially characterized in terms of its apparent Michaelis constant (k_m) value [the equilibrium NO concentration ([NO]) at which sGC is 50% activated]. Stone and Marletta (44) reported an upper limit of 250 nM for k_m. However, recent data suggest that k_m is most likely an order of magnitude lower (~23 nM; Refs. 9, 55). If k_m is on the order of 23 nM, previous estimates for the effective distance over which NO can influence the activation of sGC (49) need to be reevaluated.

Vaughn et al. (48, 49) demonstrated that the theoretical "effective diffusion distance" (defined as the distance away from its production source within which [NO] exceeds the k_m of sGC) is strongly dependent on the geometry of its source. Their results suggest that vascular endothelial cells cannot produce free NO at high enough levels to activate sGC in adjacent smooth muscle cells without the protection of an additional cofactor because of the consumption of NO by oxyhemoglobin (Hb) in blood. Their analysis considered a semi-infinite system at steady state, with k_m = 250 nM.

Expired human breath contains 4–100 ppb NO (14, 42, 43, 50). Exhaled NO has been proposed as a noninvasive biomarker for disease states characterized by inflammation, such as bronchial asthma and allergies (41–43). The potential of endothelium-derived NO to contribute significantly to the levels appearing in expired breath remains to be investigated.

EDRF is hypothesized to be either free NO or NO bound to a protective cofactor (13, 19). On the basis of in vitro data, the half-life of NO within red blood cells is ~1 μs (11, 17, 29). Thus the rapid reaction of NO with Hb present in erythrocytes suggests that other physical or chemical factors are required to activate sGC in smooth muscle cells. If free endothelium-derived NO is EDRF, how does it escape the abyss of Hb in blood vessels to perform its physiological function? One proposed hypothesis is that an erythrocyte-free zone (EFZ) is formed because of the tendency of erythrocytes to migrate away from the blood vessel wall under flow conditions. The EFZ provides a diffusion barrier between erythrocytes and the inner blood vessel wall (5, 29, 30, 48, 49). Recent studies suggest that erythrocytes regulate NO consumption via Hb by means of an intrinsic diffusion barrier at their cell

Address for reprint requests and other correspondence: S. C. George, Dept. of Chemical Engineering and Materials Science, 916 Engineering Tower, Univ. of California, Irvine, CA 92697-2575 (E-mail: scgeorge@uci.edu).

The costs of publication of this article were defrayed in part by the payment of page charges. The article must therefore be hereby marked "*advertisement*" in accordance with 18 U.S.C. Section 1734 solely to indicate this fact.

membranes (18, 47). In either case, NO uptake by Hb is limited by diffusion resistance.

We present here a simplified analytical model for small NO-producing blood vessels within the human bronchial circulation, which are bounded by the airway lumen gas space. We consider both steady-state and transient behavior for a finite geometry, predict NO concentration profiles and diffusion rates at in vivo conditions, and hypothesize possible mechanisms for free NO-modulated smooth muscle dilation. Our goal is to identify potential pathways that may govern the fate and physiological activity of endothelium-derived NO in the human bronchial circulation.

Glossary

C	NO concentration (nM)
C_i	$C(t, r = R_i)$ = NO concentration at surface; i = 1, 2, 3 (nM)
$C_{i,ss}$	Steady-state concentration at surface; i = 1, 2, 3 (nM)
$C^0_{ss}(x)$	Initial, steady-state NO concentration distribution (nM)
C_∞	Bulk fluid phase NO concentration (nM)
$C_{1,ss}$	$C(t\rightarrow\infty, y = 1)$ = steady-state NO concentration at surface; i = 1 (nM)
$C_{2,ss}$	$C(t\rightarrow\infty, y_2)$ = steady-state NO concentration at surface; i = 2 (nM)
$C'_{1-,ss}$	$\partial C/\partial y\|_{y_1^-}$ at steady state = $C_{1,ss}/[y_1 \ln (y_1/y_0)]$
$C'_{2+,ss}$	$\partial C/\partial y\|_{y_2^+}$ at steady state = $(f'_{12}/f_{12})C_{2,ss} - (g'_{12} - g_{12}f'_{12}/f_{12})Q_{1,ss} - Q_{2,ss}$
D	Diffusivity of NO within tissue (cm^2/s or $\mu m^2/s$)
$F_1(y)$	Known function of y and input parameters; i = 1, 2
f_{ij}	$f_i(y_j)$
$f'_j(y)$	$df_j(y)/dy$
f'_{ij}	$f'_i(y_j)$
$g_i(y)$	Known function of y and input parameters; i = 1, 2
g_{ij}	$g_i(y_j)$
$g'_j(y)$	$dg_j(y)/dy$
g'_{ij}	$g'_i(y_j)$
h_i	Mass transfer coefficient at boundary; i = 1, 2, 3 ($\mu m/s$)
h_3	Mass transfer coefficient between adventitial boundary and external medium ($\mu m/s$)
H_3	h_3R_1/D = dimensionless mass transfer coefficient
J_i	Molar diffusion flux at boundary i ($\mu M\cdot\mu m\cdot s^{-1}$)
k_1	First-order rate constant for NO consumption in pulmonary tissue (s^{-1})
k_m	Apparent Michaelis constant for sGC with NO as substrate (nM)
K_m	Modified Bessel function of the second kind of order m
$q_i(\tau)$	$[Q_i(\tau) - Q_i^0]/\Delta Q^{Max}$ = dimensionless endothelial NO production rate; i = 1, 2
q_i^{Max}	$(Q_i^{Max} - Q_i^0)/\Delta Q^{Max}$ = maximum dimensionless NO production rate; i = 1, 2
$Q_i(\tau)$	$\dot{S}_{NO,i}(t)R_1/D$ = scaled endothelial NO production rate; i = 1, 2 (nM)
Q_i^0	$\dot{S}^0_{NO,i}R_1/D$ = scaled endothelial NO production rate at t = 0; i = 1, 2 (nM)
Q_i^{Max}	$\dot{S}^{Max}_{NO,i}R_1/D$ = maximum scaled endothelial NO production rate; i = 1, 2 (nM)
r	Radial space coordinate (μm)
r_{eff}	Effective diffusion radius (μm)
R_0	Radius of hypothetical red blood cell core (μm)
R_1	Blood vessel radius at inner membrane surface (μm)
R_2	Blood vessel radius at outer membrane surface (μm)
R_3	Radial distance from blood vessel center to outer adventitial boundary (μm)
$R_{NO}(C)$	NO consumption rate in pulmonary tissue (nM/s) = k_1C [$R_{NO}(C) = 0$ in EFZ]
$\dot{S}_{NO,i}(t)$	Endothelial NO production rate per unit surface; i = 1, 2 ($\mu M\cdot\mu m\cdot s^{-1}$)
$\dot{S}^0_{NO,i}$	Basal endothelial NO production rate per unit surface; i = 1, 2 ($\mu M\cdot\mu m\cdot s^{-1}$)
$\dot{S}^{Max}_{NO,i}$	Maximum endothelial NO production rate per unit surface; i = 1, 2 ($\mu M\cdot\mu m\cdot s^{-1}$)
[species]	Concentration of species in tissue; species = NO, O_2 (nM)
t	Time (s)
V	Equivalent sGC activity level (cGMP formation rate) at steady state (nM/s)
V/V_{max}	Equivalent relative sGC activity level at steady state, V/V_{Max}
V_{Max}	Maximum possible cGMP formation rate (nM/s)
x_j	Input parameter j for linear regression analysis
y	r/R_1 = dimensionless radial space coordinate (relative to blood vessel radius)
y_{eff}	r_{eff}/R_1 = dimensionless effective diffusion radius
β_j (η_i)	Sensitivity coefficient (of η_i to input j) for linear regression analysis
δ	Equilibrium distribution coefficient between adventitial region and external medium
δC_∞	Driving force term (product of δ and C_∞) (nM)
ΔC_i	Concentration driving force for mass transfer at boundary; i = 1, 2 (nM)
$\Delta Q(\tau)$	$Q_1(\tau) + Q_2(\tau) - Q_1^0 - Q_2^0$
ΔQ^{Max}	$Q_1^{Max} + Q_2^{Max} - Q_1^0 - Q_2^0$
η_i	Fractional flux at surface; i = 1, 2, 3
κ^2	Theile modulus = $k_1R_1^2/D$
τ	Dt/R_1 = dimensionless time
T	Time duration of simultaneous pulse changes in NO production (s)
T_1	On-time for a continuous (square wave) pulse in NO production (s)

T_2 Off-time for a continuous (square wave) pulse in NO production (s)

Subscripts and Superscripts

0 Initial or basal condition
i Index corresponding to $r = R_1$ ($i = 1$), $r = R_2$ ($i = 2$), and $r = R_3$ ($i = 3$) or general integer
$i+$ Evaluation at the outer surface of a boundary
$i-$ Evaluation at the inner surface of a boundary
j Index corresponding to general integer; $j = 1, 2, 3$
Max Maximum
ss Steady state

METHODS OF ANALYSIS

Endothelial NO production near an arteriole. A typical geometry for a blood vessel of the bronchial circulation is depicted in Fig. 1, with the radial coordinate denoted by r. Erythrocyte(s) are assumed to be clustered at the center of the blood vessel ($r < R_0$). R_1 and R_0 denote the radii of the blood vessel and its hypothetical red blood cell (RBC) core, respectively, with the region $R_0 < r < R_1$ comprising an EFZ.

For small blood vessels, individual endothelial cells form nearly cylindrical annuli over small axial and angular distances. eNOS is a membrane-bound enzyme (54). We assume that NO is produced at the endothelial membranes, which are thin compared with the total cell thickness (see Fig. 1*B*). The NO production rates, per unit surface, at the inner ($r = R_1$) and outer ($r = R_2$) endothelial cell membranes are $\dot{S}_{NO,1}$ and $\dot{S}_{NO,2}$, respectively (49). Because the substrate, L-Arg, is a ubiquitous amino acid, we assume that [L-Arg] > [NO]. Thus $\dot{S}_{NO,1}$ and $\dot{S}_{NO,2}$ are independent of [NO]. Recent experimental data suggest that micromolar levels of NO reversibly inhibit NOS (39). However, these levels are at least two orders of magnitude higher than those considered here.

Beyond the endothelium ($R_3 > r > R_2$) lies adjacent (adventitial) tissue. Vascular smooth muscle cells (~1–8 μm diameter) lie adjacent to the endothelium of small arterioles ($R_1 \approx$ 5–100 μm). The thickness of this smooth muscle region is estimated as ~10–20% of the blood vessel radius, R_1 (4, 48, 49).

Governing equation and boundary conditions. We assume that, over limited regions of the blood vessel circumference, angular and axial diffusion rates are small compared with the radial diffusion rate. Hence, the one-dimensional diffusion equation in cylindrical coordinates applies to each region

$$\frac{\partial C}{\partial t} = \frac{D}{r}\frac{\partial}{\partial r}\left(r\frac{\partial C}{\partial r}\right) - R_{NO}(C) \qquad (1)$$

where t is time, r is the radial coordinate, C is the concentration of NO, $R_{NO}(C)$ is the NO consumption rate per unit volume, and D is the diffusivity of NO within tissue. D is estimated as the diffusivity of NO within water (i.e., $D = 3.3 \times 10^{-5}$ cm^2/s) (25, 26, 48).

The most active scavengers of NO within pulmonary tissue are most likely O_2^- and Hb (1, 14, 40, 51, 52). The reaction of NO with O_2^- is first order with respect to [NO] and occurs in the adventitial tissue, whereas its consumption by Hb occurs in the RBC core. NO consumption rates are assumed to be negligible within erythrocyte-free blood plasma, where Hb and O_2^- are absent [$R_{NO}(C) = 0$ in the EFZ]. However,

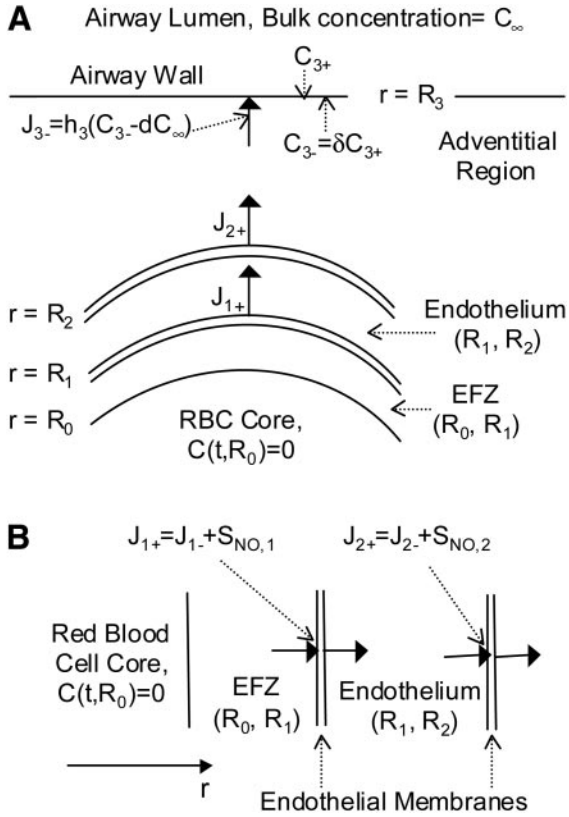

Fig. 1. Geometry and boundary conditions for a typical bronchial blood vessel. *A*: adventitial region, endothelium, erythrocyte-free zone (EFZ), and red blood cell (RBC) core. *B*: detail of blood vessel showing endothelial membranes. See *Glossary* for definitions.

irreversible oxidation of NO in RBCs is assumed to be instantaneous within the RBC core [i.e., at $r \le R_0$, $C(t, r = R_0) = 0$]. We assume first-order NO consumption within the pulmonary tissue surrounding the blood vessel, $R_{NO}(C) = k_1 C$, where k_1 is the first-order rate constant with respect to NO. *Equation 1* can be expressed in terms of dimensionless length, $y = r/R_1$, and time, $\tau = Dt/R_1^2$ (see APPENDIX). The Thiele modulus, $\kappa^2 = k_1 R_1^2/D$, is also dimensionless and corresponds to the ratio of reaction rate to diffusion rate.

The NO concentrations on each side of a boundary between adjacent tissue regions are assumed equal. However, at the inner and outer endothelial membrane surfaces ($r = R_1$ and $r = R_2$), NO production, $\dot{S}_{NO,i}(t)$, contributes to the molar diffusion flux, $J_i = (-D\partial C/\partial r)_i$, as expressed by the internal boundary condition

$$J_{i+} - J_{i-} = \dot{S}_{NO,i}(t) \quad \text{at } r = R_1 (i = 1) \text{ and } r = R_2 (i = 2) \qquad (2)$$

where the molar diffusion flux is directed outward from the NO-producing cell(s) and the subscripts $i+$ and $i-$ denote evaluation of the molar diffusion flux, J_i, at the outer and inner membrane surfaces, respectively (i.e., $r = R_1^+$ and $r = R_1^-$ or $r = R_2^+$ and $r = R_2^-$). If the NO production rate per unit surface, $\dot{S}_{NO,i}(t)$, in *Eq. 2* is zero, the concentration gradient is continuous across the boundary. The relationships implied by *Eq. 2* are based on our assumption that the cell membrane is infinitesimally thin (see Fig. 1*B*).

Non-NO-producing adventitial tissue lies external to the cell membrane boundaries. We assume that the outer adven-

titial boundary lies adjacent to a fluid (e.g., gas or blood) and impose the boundary condition

$$J_{3-} = -D\partial C/\partial r|_{R_3} = h_3[C_{3-} - \delta C_\infty] \quad \text{at } r = R_3 \qquad (3)$$

where δ is an equilibrium distribution coefficient.

C_∞ is the bulk fluid concentration (assumed constant), h_3 is the mass transfer coefficient between the adventitial boundary (2) and the external medium ($H_3 = h_3R_1/D$ in dimensionless form), and $[C_{3-} - \delta C_\infty]$ represents a driving force term. The subscript $3-$ implies evaluation at the inner surface of the outer adventitial boundary ($r = R_3^-$). This work focuses on NO transport from the blood vessel to the airway lumen gas space. Thus we determined h_3 based on theoretical gas phase mass transfer rates (8); δ is the air/tissue equilibrium partition coefficient (35a), and C_∞ is the bulk gas phase concentration.

Fractional mass transfer flux. We define the fractional flux, η_i, as the mass flux across a boundary i relative to the total endothelial NO production rate. For a cylindrically shaped blood vessel, where $\dot{S}_{NO,i}$ is uniform over each membrane surface ($i = 1, 2$)

$$\eta_i = \frac{|(-D\partial C/\partial_r|_i)R_i|}{\dot{S}_{NO,1}R_1 + \dot{S}_{NO,2}R_2} = \frac{|(-\partial C/\partial y|_i)y_i|}{Q_1 + Q_2y_2}$$
$$i = 1-, 2+, \text{ or } 3- \qquad (4)$$

where $y_i = R_i/R_1$ ($i = 1, 2, 3$) and $Q_i = \dot{S}_{NO,i}R_1/D$ ($i = 1, 2$) denote the scaled production rates. *Equation 4* assumes that J_i is directed normal to surface i and away from the endothelial cell. If the diffusive flux is directed into the endothelial cell, $\eta_i < 0$. There is no accumulation of NO within the endothelial cell at steady state; therefore $\eta_{1-} + \eta_{2+} = 0$. At the outer boundary of the adventitial region ($i = 3-$ and $r = R_3^-$), computation of η_{3-} from *Eq. 4* is valid over a limited region of the blood vessel circumference, where the angular flux contribution is negligible. Henceforth, we denote η_{1-}, η_{2+}, and η_{3-} as η_1, η_2, and η_3 or η_i ($i = 1, 2, 3$), respectively.

Steady-state analysis. When both the external conditions and the NO production rates remain unchanged for a long time, the time derivative in *Eq. 1* vanishes and the steady-state solution can be derived by integration of the resulting ordinary differential equation (see APPENDIX). Although this yields a complex system of algebraic expressions, values of η_i are readily computed from *Eq. 4*.

At steady state, η_i ($i = 1, 2, 3$) values depend on seven specified parameters (k_1, $y_0 = R_0/R_1$, $y_2 = R_2/R_1$, $y_3 = R_3/R_1$, R_1, δC_∞, and h_3) but are independent of the NO production rates. Also, at steady state, there is no accumulation of NO in the endothelium and $\eta_1 + \eta_2 = 1$ (i.e., the total flux entering both blood and surrounding tissue equals the NO production rate within the endothelium). Thus only η_2 and η_3 need to be considered in this analysis, and we treat η_i ($i = 2, 3$) as output parameters dependent on the specified (input) parameters, which are treated as independent variables. The mean values and ranges of the input parameters are summarized in Table 1. We estimated EFZ thickness, $R_1 - R_0$, and representative probability distributions on the basis of experimental measurements of vascular hematocrit as a function of blood vessel radius at typical blood velocities (4, 27, 48, 49). Thus these estimates account for the Fahreus effect. We assumed NO production rates of $\dot{S}_{NO,1,ss} = \dot{S}_{NO,2,ss} = 26.5$ $\mu M \cdot \mu m \cdot s^{-1}$ for this analysis, on the basis of published data (33, 48). Because, at steady state, η_2 and η_3 are dependent only on the ratio $\dot{S}_{NO,1,ss}/\dot{S}_{NO,2,ss}$ and independent of the magnitude of NO production, we did not study $\dot{S}_{NO,1,ss}$ and $\dot{S}_{NO,2,ss}$ as input parameters.

Table 1. *Input parameter ranges for steady-state regression analysis*

Parameter	Units	Lower Limit	Mean Value	Upper Limit	References
k_1[a]	s^{-1}	0.05	0.35	1.5	14, 25, 33, 53
$y_0 = R_0/R_1$[b]		0.70	0.80	0.95	4, 27, 48, 49
$y_2 = R_2/R_1$[c]		1.05	1.25	1.5	4, 48, 49
$y_3 = R_3/R_1$[d]		2	6	20	4, 6, 12, 28
R_1[e]	μm	3	10	20	6, 28
δC_∞[f]	nM	0	0.16	0.7	46
h_3[g]	$\mu m/s$	3×10^5	1×10^6	6×10^6	2, 8

[a]Based on 0.5- to 15-s half-life (14, 25, 33, 53); [b]$y_1 \approx 0.95$ (large blood vessels) (48, 49) to 0.7 (capillaries of 10-μm diameter corresponding to 50% hematocrit) (4, 27); [c]endothelium thickness, ($R_2 - R_1$), range: 0.2 μm for capillaries (5) to 10 μm for large blood vessels (48, 49); [d]based on conductive airway epithelial thickness with generation number (4, 8, 12, 28); [e]based on morphological data for the bronchial circulation (6, 28); [f]based on endogenous NO concentrations predicted in conductive airway lumen (46); [g]based on theoretical mass transfer coefficients predicted for the human conductive airways (2, 8). See *Glossary* for definitions.

To simplify the complex form of the steady-state solution, the dependence of η_i ($i = 2, 3$) on the specified parameters is assessed by linear regression analysis, with input parameter values selected by Latin hypercube sampling (LHS) (34). Thus we correlate η_i to the form $\eta_i = \Sigma\beta_j(\eta_i)x_j$, where x_j and $\beta_j(\eta_i)$ denote the input parameters and sensitivity coefficients of the output, η_i, respectively. The purpose of this analysis is to identify trends, which represent the dependence of η_i on the input parameter values specified in the simulations. *P* values, which correspond to the probabilities that either η_i is independent of a particular x_j, provide a quantitative assessment of the significance of the dependence of η_i on each input parameter. Thus we calculate rigorous results with our relatively complex mathematical model and attempt to identify the most important input parameters with regression analysis.

Transient analysis. The transient solution of *Eq. 1* is obtained by the method of separation of variables, which leads to an infinite series of Bessel functions in the radial space coordinate (7, 15, 38). The solution is expressed as the sum of steady-state and transient parts (see APPENDIX).

The initial steady-state concentration distribution corresponds to the basal NO production rates, $\dot{S}^0_{NO,i}$ ($i = 1, 2$). Transient computations consider abrupt changes in $\dot{S}_{NO,i}$ from $\dot{S}^0_{NO,i}$ to their maximum values, $\dot{S}^{Max}_{NO,i}$, at time $t = 0$. Identical changes in $\dot{S}_{NO,i}(t)$ are assumed to occur simultaneously for $i = 1$ and $i = 2$. Maximum NO production rates are estimated as $\dot{S}^{Max}_{NO,1} = \dot{S}^{Max}_{NO,2} = 26.5$ $\mu M \cdot \mu m \cdot s^{-1}$, based on published data (33, 48). Basal NO production rates are estimated as the steady-state levels required to maintain $[NO] \approx 0.2$ nM (1% sGC activation) within the vascular smooth muscle ($\dot{S}^0_{NO,1} = \dot{S}^0_{NO,2} = 0.1$ $\mu M \cdot \mu m \cdot s^{-1}$). The transient solution is expressed in terms of the dimensionless NO production rates, $q_i(\tau) = [\dot{S}_{NO,i}(t) - \dot{S}^0_{NO,i}]/(\dot{S}^{Max}_{NO,1} + \dot{S}^{Max}_{NO,2} - \dot{S}^0_{NO,1} - \dot{S}^0_{NO,2})$, which may be arbitrary functions of time (15). The maximum values of $q_i(\tau)$ satisfy $q_1^{Max} + q_2^{Max} = 1$.

Three NO production scenarios are considered. The "step change" scenario considers a single abrupt simultaneous change in $\dot{S}_{NO,i}(t)$ from $\dot{S}^0_{NO,i}$ to $\dot{S}^{Max}_{NO,i}$ at $t = 0$. The "single pulse change" scenario considers abrupt, simultaneous changes in $\dot{S}_{NO,i}(t)$ from $\dot{S}^0_{NO,i}$ to $\dot{S}^{Max}_{NO,i}$ at $t = 0$ and from $\dot{S}^{Max}_{NO,i}$ to $\dot{S}^0_{NO,i}$ at $t = T$ (pulse duration time). In the "continuous pulse" (square wave) scenario, $\dot{S}_{NO,i}(t)$ values are maintained at $\dot{S}^{Max}_{NO,i}$ and $\dot{S}^0_{NO,i}$ over time intervals T_1 and T_2,

respectively, with abrupt changes between these two extremes to form a square-wave pattern with this cycle repeating indefinitely. The time intervals T_1 and T_2 are referred to as the pulse "on-time" and "off-time," respectively. The transient response for this scenario is evaluated after a relatively long time ($t > 20$ s). T_1 and T_2 were selected as 500 ms and 5 s, respectively, on the basis of previously published experimental data (22, 33, 36, 55) and previously published simulations of these data (9, 24–26, 48, 49, 53). These data and simulations demonstrated that sGC activation by NO is at least an order of magnitude faster than its deactivation via NO dissociation (i.e., 5 s/500 ms = 10) and suggested that NO may exert its physiological influence within seconds of its generation.

We define the effective diffusion radius, r_{eff}, as the radial distance away from the blood vessel within which [NO] exceeds the k_m value corresponding to 50% sGC activation (49). These results are expressed as the scaled effective diffusion radius, $y_{eff} = r_{eff}/R_1$. We convert [NO] to equivalent relative sGC activity level at steady state, V/V_{max}, on the basis of previous work, which determined a k_m of ~23 nM and a Hill coefficient of 1.3 (9, 55). Thus basal (1%), 10%, 50%, and 90% sGC activity levels are assumed at [NO] ≈ 0.2, 4, 23, and 100 nM, respectively.

RESULTS

Steady-state analysis. Table 2 summarizes the results of LHS linear regression analysis in terms of the *P* values and regression coefficients, which are indices of the significance and sensitivity, respectively, with respect to the corresponding input parameters. Both η_2 and η_3 are more sensitive to y_0, y_2, and y_3 than the other parameters, as demonstrated by their low *P* values and high regression coefficients (see Table 2); η_2 is weakly dependent on both R_1 and k_1. Unlike η_2, η_3 decreases with k_1 and is not significantly dependent on R_1.

The dependence of η_2 on y_0, y_2, and y_3 with $R_1 = 10$ μm is depicted in Fig. 2. The results shown in Fig. 2 are consistent with the regression coefficients shown in Table 2 (η_2 increases with y_2, decreases with y_0, and decreases with y_3 at fixed y_0). Although η_2 increases with both R_1 and k_1 (see Table 2), this subtle dependence is not depicted in Fig. 2. The dependence of η_3 on the same input parameters (see Fig. 3) shows behavior analogous to that of η_2. As a result of chemical consumption, $\eta_3 < \eta_2$ for fixed values of the input parameters (compare Figs. 2 and 3).

Over the range of input parameter values considered in this study, computed values of η_3 and η_2 varied between 0.01 and 0.9 (data simulations not shown). However, as depicted in Figs. 2 and 3, an upper limit of 0.4–0.6 for η_3 is probably more realistic under most scenarios of physiological interest. For an arteriole, which is located very close to the airway lumen, this suggests that, at most, 40–60% of the produced NO will reach the air space. We emphasize that this may still be negligible compared with the contributions of other NO-producing tissue, such as the bronchial epithelium.

The steady-state dependence of the dimensionless effective diffusion radius, $y_{eff} = r_{eff}/R_1$, on the blood vessel radius, R_1, is shown in Fig. 4. In this analysis, the other input parameters were fixed at their mean values (see Table 1). y_{eff} goes through a maximum of approximately five blood vessel radii at $R_1 = 27$ μm (see Fig. 4). This result is consistent with previous work, which predicts maximum effective diffusion distances at microvessel diameters of 30–100 μm (49). We selected the nominal value, $R_1 = 20$ μm, as the near-optimal blood vessel radius for our transient analysis. This size is within the observed range for blood vessels in the bronchial circulation (4, 6, 28).

Transient analysis. The results presented in Figs. 5–7 were computed with all input parameters set at their mean values (see Table 1) and the airway lumen outer adventitial boundary condition, unless otherwise indicated. We express transient NO concentration profiles in terms of equivalent relative sGC activity level at steady state, V/V_{Max}. For step changes in the NO production at $R_1 = 5$ and 20 μm, the dependence of V/V_{Max} on R_1 is significant (compare Fig. 5, *A* and *B*). Figure 5 shows two V/V_{Max} peaks for both 0.01 and 0.1 ms (Fig. 5*A*; $R_1 = 5$ μm) and 0.1 and 1 ms (Fig. 5*B*; $R_1 = 20$ μm). These peaks correspond to the two NO sources at the inner and outer endothelial membranes and have a "Gaussian" appearance, because at these small times very little NO has reached the RBC core and outer adventitial boundary sinks. Within 50 ms, sGC activity levels in the vascular smooth muscle region reach 45–50% ($r \approx 6$–7 μm) for $R_1 = 5$ μm (Fig. 5*A*) and 70–80% ($r \approx 24$–28 μm) for $R_1 = 20$ μm (Fig. 5*B*). Because sGC activity level is dependent on $\dot{S}_{NO,i}^{Max}$, this analysis should be revisited when more information pertaining to in vivo NO production rates becomes available.

Figure 6 depicts the time dependence of the fractional fluxes with $R_1 = 20$ μm. The other input param-

Table 2. *Steady-state regression analysis from Latin hypercube sampling*

Input *j*	Output Parameter		η_2		η_3	
	Units	Range	*P* value	Coefficient $\beta_j(\eta_2)$	*P* value	Coefficient $\beta_j(\eta_3)$
k_1	s^{-1}	0.05–1.5	3.0×10^{-3}	0.009	7.4×10^{-6}	−0.016
$y_0 = R_0/R_1$		0.70–0.95	1.5×10^{-49}	−0.571	1.0×10^{-41}	−0.533
$y_2 = R_2/R_1$		1.05–1.5	7.2×10^{-36}	0.256	2.6×10^{-28}	0.234
$y_3 = R_3/R_1$		2–20	7.0×10^{-32}	−0.005	1.2×10^{-40}	−0.008
R_1	μm	3–20	5.2×10^{-3}	0.003	0.57	−0.001
δC_∞	nM	0–0.7	0.48	−0.005	0.22	−0.010
h_3	μm/s	3×10^5–6×10^6	0.51	5×10^{-10}	0.34	8×10^{-10}

See Table 1 for references and *Glossary* for definitions.

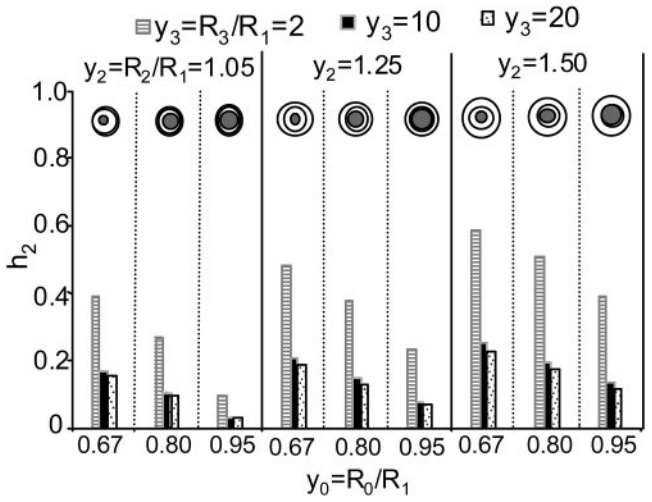

Fig. 2. Fractional flux η_2 at the outer blood vessel surface with inner blood vessel radius (R_1) = 10 μm, mass transfer coefficient (h_3) = 1×10^6 μm/s, and driving force term (δC_∞) = 0.16 nM.

eters were fixed at their mean values (see Table 1). For $t < 200$ ms η_3 is very small, but for $t > 2$ s $\eta_3 \rightarrow \eta_2$. Hence, ~100 ms is required for the NO signal to reach the outer adventitial boundary. For $t < 10$ ms $\eta_1 < \eta_2$ and $\eta_1 + \eta_2 < 1$, whereas for $t > 2$ s $\eta_1 \rightarrow 0.83 > \eta_2 \rightarrow 0.16$ and $\eta_1 + \eta_2 \rightarrow 1$. This behavior results from the combined effects of NO accumulation in the endothelium and the finite transit time required for NO diffusion from the inner wall of the blood vessel to the RBC core.

For a step change in NO production with R_1 = 20 μm, V/V_{Max} reaches 85–90% equivalent (steady state) sGC activity in the vascular smooth muscle region ($r \approx$ 24–28 μm) within 500 ms (Fig. 5*B*). This implies that if [NO] is maintained at the levels achieved after 500 ms, sGC present in vascular smooth muscle will eventually reach 85–90% of its maximum activity. Figure 7 compares V/V_{Max} for pulses of the same amplitude and

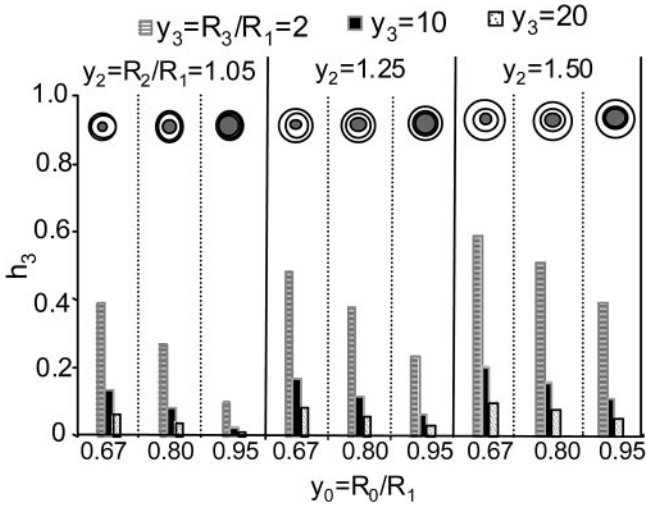

Fig. 3. Fractional flux η_3 at the airway lumen boundary with R_1 = 10 μm, $h_3 = 1 \times 10^6$ μm/s, and δC_∞ = 0.16 nM. *y*, Dimensionless radial space coordinate.

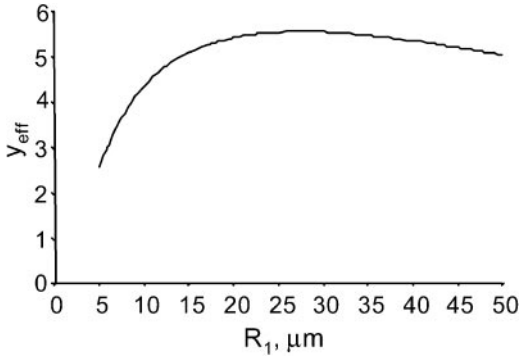

Fig. 4. Effective diffusion distance, y_{eff}, at steady state.

duration with R_1 = 20 μm. For a single pulse of duration, T = 500 ms (see Fig. 7), the same activity level is achieved. After the pulse is "turned off" at t = 500 ms, V/V_{Max} drops to near-basal levels within 5 s. The transient responses for continuous (square wave) pulses with an on-time of T_1 = 500 ms and an off-time of T_2 = 5 s were virtually identical to those depicted in Fig. 7 for a single pulse (data simulations not shown). Thus the results shown in Fig. 7 apply to both the single-pulse and square-wave pulse scenarios.

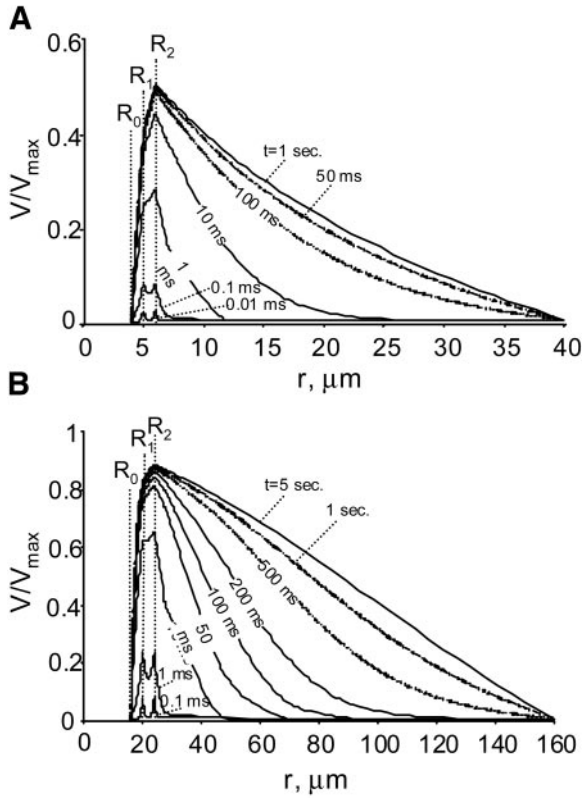

Fig. 5. Radial profiles of soluble guanylate cyclase (sGC) activity, V/V_{max}, with time, *t*, for a step increase in nitric oxide (NO) production rate. k_1, $y_0 = R_0/R_1$, $y_2 = R_2/R_1$, $y_3 = R_3/R_1$, $h_3 = 1 \times 10^6$ μm/s, and δC_∞ are at the mean values listed in Table 1, and the maximum NO production rates are $\dot{S}^{Max}_{NO,1} = \dot{S}^{Max}_{NO,2} = 26.5$ μM·μm·s^{-1}. *A*: R_1 = 5 μm. *B*: R_1 = 20 μm.

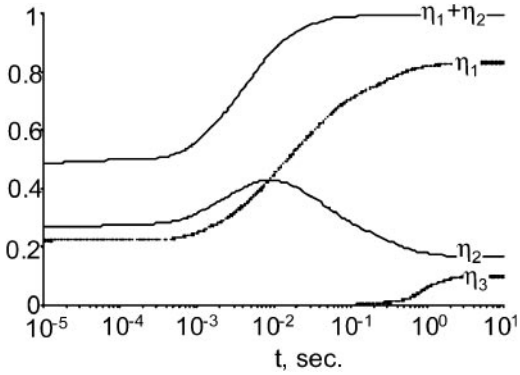

Fig. 6. Fractional fluxes at blood vessel and airway lumen surfaces. R_1 = 20 μm; k_1, $y_0 = R_0/R_1$, $y_2 = R_2/R_1$, $y_3 = R_3/R_1$, $h_3 = 1 \times 10^6$ μm/s, and δC_∞ are at the mean values listed in Table 1, and $\dot{S}^{Max}_{NO,1} = \dot{S}^{Max}_{NO,2} = 26.5$ μM·μm·s^{-1}.

DISCUSSION

We have computed theoretical concentration profiles and diffusion rates around NO-producing blood vessels based on a mathematical model applicable to the human pulmonary system. Our results confirm that endothelium-derived free NO is capable of modulating vascular smooth muscle tone by activation of sGC. We hypothesize that intermittent generation of NO by eNOS may minimize losses to blood and surrounding tissue. In addition, we cannot rule out a potential contribution of eNOS to the levels of NO appearing in expired breath.

Several mathematical models have been used to study in vivo NO diffusion. The point source model (24–26, 53) assumes that the physical dimensions of each source (NO-producing cell) are small compared with the surrounding medium and sums up all contributions from multiple sources. For a single point source, which generates NO for 1–10 s, this model predicts that the "physiological sphere of influence" is ~200 μm away from its source, provided the half-life of NO within tissue is <5 s. These results led to the hypothesis that, with the exception of blood, chemical consumption of NO in most tissues is slow compared with its diffusion rates.

Vaughn et al. (48, 49) estimated effective diffusion distances for endothelial NO production in blood vessels. Their model accounted for the finite geometry of the production source. However, their analysis was limited to the steady-state behavior of a semi-infinite system, and they assumed k_m = 250 nM for sGC activation (44). Their results demonstrate the significant influence of blood vessel geometry and rapid binding of NO to Hb in blood. They suggested that free NO produced by vascular endothelial cell(s) cannot escape consumption by Hb and still activate sGC in vascular smooth muscle cells without the protection of an additional cofactor.

Under flow conditions, NO consumption by erythrocytes proceeds at a slower rate than that observed in the presence of free Hb (29, 47). Proposed explanations for this slower consumption rate include the diffusion resistance of the EFZ (devoid of erythrocytes) around the RBC core (30) and formation of relatively stagnant (unstirred) plasma layers around individual erythrocytes within the RBC core (32). Alternately, the possibility that a cytoskeletal network of proteins adjacent to the cell membranes of erythrocytes provides additional resistance to NO diffusion has also been proposed (18). Each of the above hypotheses suggests that an additional diffusion barrier limits consumption of NO by erythrocytes. Our model approximates this additional mass transfer resistance as an annular ring of erythrocyte-free plasma around a central RBC core.

Recent evidence suggests that $k_m \approx$ 23 nM, an order of magnitude lower than the upper limit of 250 nM reported by Stone and Marletta (Ref. 44; see Refs. 9, 55). On the basis of these data, we expressed NO concentrations in terms of sGC activity level, V/V_{Max} (Figs. 5 and 7), and reevaluated the effective diffusion distance at steady state (Fig. 4). The incorporation of a finite external boundary provides additional impetus for mass transport away from the blood vessel. Although our model assumes zero [NO] at the outer boundary of a central RBC core, we include additional diffusion resistance resulting from the EFZ thickness, which is consistent with current experimental data. Our results suggest that the EFZ substantially limits NO consumption by Hb and is potentially a major contributor to the effectiveness of free NO as a vasodilator.

Our results suggest that the above considerations are sufficient for free NO to perform its physiological role of vasodilation in smooth muscle. However, although 45–80% of full sGC activity is achieved in vascular smooth muscle at steady state, ~80% of the produced NO diffuses into the blood vessel (see Figs. 5 and 6). The time dependence of NO production provides a potential mechanism for enhanced utilization of NO for smooth muscle dilation (Figs. 6 and 7). At short times, these transient concentration profiles have Gaussian shapes as NO accumulates within the endothelium. Under these conditions, large concentra-

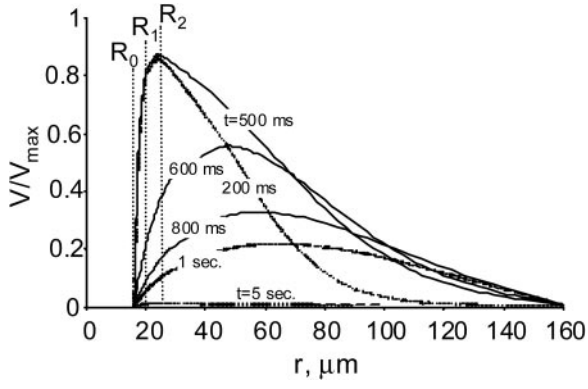

Fig. 7. Radial profiles of sGC activity, V/V_{max}, with time, t, for both single pulse [pulse duration time (T) = 0.5 s] and square-wave pulse [pulse on-time (T_1) = 0.5 s; pulse off-time (T_2) = 5 s] increases in NO production rate. R_1 = 20 μm; k_1, $y_0 = R_0/R_1$, $y_2 = R_2/R_1$, $y_3 = R_3/R_1$, $h_3 = 1 \times 10^6$ μm/s, and δC_∞ are at the mean values listed in Table 1, and $\dot{S}^{Max}_{NO,1} = \dot{S}^{Max}_{NO,2} = 26.5$ μM·μm·s^{-1}.

tion changes take place over a very thin region. Thus initial NO diffusion rates, both into and away from the blood vessel, are roughly equal and are virtually unaffected by external boundaries (Figs. 5 and 6). Transient concentration profiles strongly depend on the blood vessel radius, R_1 (Fig. 5). For a near-optimal blood vessel radius, $R_1 = 20$ μm and $\dot{S}^{Max}_{NO,1} = \dot{S}^{Max}_{NO,2} = 26.5\ \mu M \cdot \mu m \cdot s^{-1}$ (48), 60–80% of full sGC activation can be achieved in vascular smooth muscle within 50–100 ms (Fig. 5*B*).

With $R_1 = 20$, we compared V/V_{Max} for step, single-pulse, and continuous (square wave) pulse changes in NO production rate. Our results show that pulsatile generation of NO via eNOS results in enhanced utilization of NO for smooth muscle dilation. Square-wave and single-pulse changes in NO production achieve sGC activity levels of amplitude equal to that of the corresponding step change case (compare Figs. 5*B* and 7). However, the time-weighted average NO production rate for the square-wave case is only 10% of that for the corresponding step change case. The enhanced utilization efficiency results from reduced NO losses to Hb in the blood vessel.

Analysis of in vitro data demonstrates that activation of sGC by NO is rapid compared with its NO dissociation from sGC. Dissociation proceeds with a half-life of ~1–2 min (3, 9, 19, 22, 23, 36). However, sGC activation is at least an order of magnitude faster. Despite limited capacity, the initial binding rate of NO to sGC in smooth muscle is nearly as rapid as its binding rate with Hb in blood (9, 55). Thus NO binds to sGC, present in smooth muscle (at high [NO] with maximum NO production rate, $\dot{S}^{Max}_{NO,i}$), much faster than it dissociates (at low [NO] with basal NO production, $\dot{S}^{0}_{NO,i}$). Therefore, if NO is generated in brief, intermittent bursts, diffusion rates away from the source are virtually identical in both directions and comparable amounts of NO bind to both sGC and Hb. When [NO] is high, sGC is rapidly converted into to the activated state. However, when NO production is "turned off", [NO] decreases, but dissociation is so slow that most of the sGC remains in the activated state and does not approach the basal state for 1–2 min. Our model results depict a scenario in which V/V_{Max} reaches ~80% within 500 ms and the next "pulse" of NO production reaches adjacent smooth muscle 5 s later, thereby maintaining sGC in the activated state. Thus $T_1 = 500$ ms and $T_2 = 5$ s represent a near-optimal NO utilization efficiency.

Temporal changes in shear stress and circumferential strain typically occur over time scales on the order of 1 s. These changes impose dynamic forces on vascular endothelial cells and impact NO production rates (35, 37). Therefore, cyclic changes in vascular stress and strain could trigger endothelial NO production according to the scenario described above. In addition, muscular contraction and relaxation have been shown to exhibit cyclic behavior with periods of <1 s. (21). Because NO remains bound to sGC for at least several seconds, a periodic NO signal would eventually force sGC into the activated state. Therefore, we hypothesize that pulsatile changes in blood flow actuate bursts of NO production over time scales on the order of seconds, which are capable of essentially full sGC activation.

At steady state, the fractional fluxes at the endothelial membranes are dependent on the endothelial and EFZ thicknesses (see Table 2 and Fig. 2). If the distance of the blood vessel from the outer adventitial boundary (characterized by y_3 and the blood vessel radius) is large, η_2 is also dependent on k_1 but essentially independent of y_3. Conversely, if the distance from the adventitial boundary is small, this dependence reverses (η_2 is independent of k_1 but dependent on y_3). At fixed y_3, as R_1 increases the distance from the outer adventitial boundary, $R_3 = y_3 R_1$, also increases. Hence, the further the blood vessel is from the outer adventitial boundary, the more time a diffusing molecule of NO has to react with scavengers in pulmonary tissue. As R_3 increases, increased NO consumption in the adventitial region results in a steeper concentration gradient and therefore a higher molar flux at the source ($r = R_2$), which leads to a higher value for η_2. Thus, for small values of R_1, η_2 is more sensitive to y_0, y_2, and y_3 than the rate constant, k_1. As R_1 increases the dependence of η_2 on k_1 becomes more significant, and η_2 becomes independent of y_3 as R_3 becomes large.

The molar flux estimated at the external boundary (characterized by η_3) is lower than the flux determined at the generating source (characterized by η_2). In contrast to η_2, η_3 is essentially independent of R_1 and exhibits greater dependence on k_1 than η_2. In addition, as k_1 increases, η_2 increases whereas η_3 decreases with increased adventitial NO consumption (compare P values and regression coefficients of 7.4×10^{-6} and -0.016 for η_3 vs. 3.0×10^{-3} and 0.009 for η_2, respectively, in Table 2). Thus NO consumption enhances mass transport at the production source ($r = R_2$) and attenuates mass transport at the outer adventitial boundary ($r = R_3$). Hence, as one moves further from the NO source, both the NO concentration and the molar flux become attenuated as a result of NO consumption by scavengers.

Table 2 also shows that both η_2 and η_3 are very sensitive to y_0, y_2, and y_3 (i.e., the ratios R_0/R_1, R_2/R_1, and R_3/R_1, respectively) but not appreciably sensitive to R_1. Hence, η_2 and η_3 are determined primarily by the relative differences $1 - y_0 = (R_1 - R_0)/R_1$, $y_2 - 1 = (R_2 - R_1)/R_1$, and $y_3 - 1 = (R_3 - R_1)/R_1$, which define the geometry of the EFZ, rather than by the luminal radius of the vessel. Thus the relative distances (and therefore the mass transfer resistances) between the NO production sources (at $r = R_1$ and R_2, respectively) and their closest sinks (at $r = R_0$ and R_3, respectively) control fluxes η_2 and η_3.

For most of our simulations, inner blood vessel radius, R_1, is large relative to the differences $R_1 - R_0$ and $R_2 - R_0$. Therefore, near the blood vessel, the effects of curvature are small and it can be modeled as if it were two flat plates. Thus η_2 is weakly dependent on R_1 and is controlled almost exclusively by y_0, y_2, and y_3. At the outer adventitial boundary ($r = R_3^-$), this "flat plate approximation" is not valid. However, for most of our

simulations, $R_3 > R_1$, and the blood vessel looks like a "point source" of NO. Thus η_3 is very insensitive to R_1 and is controlled almost exclusively by y_0, y_2, and y_3.

As one moves away from the blood vessel, angular and axial diffusion fluxes become more important. Thus the accuracy of the predicted molar flux at the outer adventitial boundary is limited. However, this model does provide an estimate for the maximum possible flux over limited regions of a blood vessel's circumference. On this basis, blood vessels must be relatively close to the airway lumen to contribute significant amounts of NO to the airway lumen gas space. For example, with $y_3 = 2$ (i.e., within 2 blood vessel radii of the airway lumen), η_3 is in the range 0.2–0.65 for $y_2 = 1.2$ (see Fig. 3). However, if the blood vessel is far away from the airway lumen, η_3 is much lower (e.g., with $y_3 = 20$, typical of the upper conductive airways of the lungs, $\eta_3 < 0.2$; see Fig. 3). Therefore, our results do not contradict the prevailing hypothesis that blood vessels do not contribute significantly to endogenous exhaled NO.

For the typical conditions assumed here, optimal NO signaling efficacy is anticipated for a blood vessel radius of ~20–30 μm (Fig. 4). The optimal blood vessel radius represents a dynamic balance between in vivo chemical consumption and NO production rates. For similar geometries, with the dimensionless length parameters, $y_i = R_i/R_1$, constant, the influence of chemical consumption and NO production increase with $\kappa^2 = k_1R_1^2/D$ and $Q_i = \dot{S}_{NO,i}R_1/D$, respectively. Thus the optimal radius corresponds to a critical blood vessel geometry at which these two opposing effects balance each other.

Thomas et al. (45) report that the half-life for NO surrounding a vessel is inversely proportional to O_2 concentration, which implies that NO consumption via its reaction with O_2 is first-order with respect to $[O_2]$. Because $[O_2]$ decreases with distance from an arteriole, a gradient (corresponding decrease) in NO consumption rate with distance from the vessel is created. Because this reaction rate is second order with respect to [NO], it would be higher at high [NO] (and lower at low [NO]) than the rate that would be predicted by a first-order mechanism. Thus we expect the apparent first-order rate constant for NO consumption to decrease as we move away from an arteriole, as proposed by Thomas et al. (45). This implies that the NO consumption rate close to the blood vessel would be faster than that predicted by a first-order mechanism and, conversely, slower as we move away from the blood vessel. This effect would "flatten" the [NO] profile, thereby decreasing the diffusion rate away from the blood vessel. The rate of NO consumption via O_2 in pure water is very slow (1), and we expect its impact to be modest. However, NO consumption via O_2 may be accelerated within the hydrophobic interiors of neighboring cell membranes (31).

In conclusion, the rapid rate of reaction of free NO with Hb in blood does not prevent its action as an important signaling molecule for vascular smooth muscle dilation. Steady-state sGC activities of 45–80% are achieved in vascular smooth muscle adjacent to 20- to 100-μm diameter arterioles. Intermittent generation of endothelial NO provides a possible mechanism to enhance sGC activation by minimizing NO losses to the blood. The latter hypothesis is deemed plausible because both pulsatile changes in vascular networks and muscular contraction/relaxation have been shown to exhibit cyclic behavior with periods of <1 s (21, 35, 37). However, experimental validation of this transient mechanism will require real-time monitoring of NO concentration at resolutions on the order of milliseconds.

APPENDIX

Dimensionless form of governing equation and boundary conditions. The transient boundary value problem of *Eqs. 1*, *2*, and *3* is expressed in dimensionless form as

$$\frac{\partial C}{\delta \tau} = \frac{1}{y}\frac{\partial}{\partial y}\left[y\frac{\partial C}{\partial y}\right] - R_1^2 R_{NO}(C)/D \qquad (A1)$$

$$C(t, y = y_0) = 0 \quad \text{at } y = y_0 = R_0/R_1 \qquad (A2)$$

$$\partial C/\partial y|_{y=1-} - \partial C/\partial y|_{y=1+} = Q_1 \quad \text{at } y_1 = 1 \qquad (A3)$$

$$\partial C/\delta y|_{y=y_2^-} - \partial C/\partial y|_{y=y_2^+} = Q_2 \text{ at } y = y_2 = R_2/R_1 \qquad (A4)$$

$$\partial C/\partial y|_{y=y_3} + H_3 C(t, y = y_3) = H_3 \delta C_\infty \quad \text{at } y = y_3 = R_3/R_1 \qquad (A5)$$

where $y = r/R_1$, $\tau = Dt/R_1$, $\kappa^2 = k_1R_1^2/D$, and $H_3 = h_3R_1/D$. $Q_i = \dot{S}_{NO,i}R_1/D$ ($i = 1, 2$) are the scaled production rates. $R_1^2R_{NO}(C)/D = \kappa^2 C$ in pulmonary tissue ($y_3 \geq y > y_1 = 1$), and $R_{NO}(C) = 0$ in the EFZ ($1 \geq y \geq y_0$). The initial condition, at $t = 0$, corresponds to steady state with basal NO production levels, $\dot{S}^0_{NO,1}$ and $\dot{S}^0_{NO,2}$, at the endothelial membrane surfaces.

Steady-state solution. At steady state (ss) the time derivative in *Eq. A1* vanishes and its solution is determined by direct integration of the resulting ordinary differential equation to obtain the following general solution

$$C_{ss}(y) = C_{1,ss} \ln(y/y_0)/\ln(1/y_0) \quad \text{EFZ } (1 \geq y \geq y_0) \qquad (A6)$$

$$C_{ss}(y) = f_1(y)C_{1,ss} - g_1(y)Q_{1,ss}$$
$$\text{endothelial cell(s) } (y_2 \geq y \geq y_1 = 1) \qquad (A7)$$

$$C_{ss}(y) = f_2(y)C'_{2+,ss} - g_2(y)\delta C_\infty$$
$$\text{adventitial region } (y_3 \geq y \geq y_2) \qquad (A8)$$

where $Q_{1,ss} = \dot{S}_{NO,1,ss}R_1/D$. $C_{1,ss} = C(t\to\infty, y = 1)$ and $C'_{2+,ss} = \partial C/\partial y|_{y_2^+}$ are known functions of the input parameters but are independent of the radial coordinate, y. $f_1(y)$, $f_2(y)$, $g_1(y)$, and $g_2(y)$ are known functions of both y and the input parameters, which satisfy *Eqs. A2–A5*, and are expressed in terms of Bessel functions.

Transient solution. We apply the method of separation of variables to obtain solutions to the governing equations, which are expressed in terms of exponential functions of time and Bessel functions in r (7, 15, 38). We then convert the resulting boundary value problem into Sturm-Louiville form, by expressing the solution as the sum of steady-state and transient parts. Application of Duhamel's principle leads to analytical solution in terms of $\dot{S}^0_{NO,i}(t)$ ($i = 1, 2$) (15).

The initial concentration distribution, $C^0_{ss}(y)$, is assumed to be the steady state corresponding to $\dot{S}_{NO,i}(t = 0) = \dot{S}^0_{NO,i}$ ($i = 1, 2$). Initially, we assume abrupt, simultaneous (step or pulse) changes in $\dot{S}_{NO,i}(t)$, from $\dot{S}^0_{NO,i}$ to $\dot{S}^{Max}_{NO,i}$, at both endothelial cell membranes ($i = 1, 2$). Thus the scaled pro-

duction rates, $Q_i(\tau) = \dot{S}_{NO,i}(t)R_1/D$, have initial and final values Q_i^0 and Q_i^{Max}, evaluated at $\dot{S}_{NO,i}^0$ and $\dot{S}_{NO,i}^{Max}$, respectively. We define the scaled change in total NO production as: $\Delta Q(\tau) = Q_1(\tau) + Q_2(\tau) - Q_1^0 - Q_2^0$, with the maximum value, ΔQ^{Max}, evaluated at Q_1^{Max} and Q_2^{Max}. Thus the dimensionless changes in NO production rates are $q_i(\tau) = [Q_i(\tau) - Q_i^0]/\Delta Q^{Max}$. Hence, the maximum values of $q_i(\tau)$ are $q_i^{Max} = (Q_i^{Max} - Q_i^0)/\Delta Q^{Max}$, where $q_1^{Max} + q_2^{Max} = 1$. Finally, we express the dimensionless concentration as $\Phi(\tau, y) = [C(t, y) - C_{ss}^0(y)]/\Delta Q^{Max}$.

For step changes in $q_i(\tau)$ the final, steady-state distribution, $\Phi_{ss}(y) = \Phi(\tau \rightarrow \infty, y)$, is determined within the three physiological regions of interest [the EFZ, endothelial cell(s), and the adventitial region] as a set of algebraic equations, which are linear in the inputs, q_1^{Max} and q_2^{Max}. Employing superposition, we set $\Phi(\tau,y) = \Phi_{ss}(y) + \Delta\Phi(\tau,y)$, substitute this sum into *Eqs. A1–A5*, and force $\Phi_{ss}(y)$ to satisfy *Eqs. A2–A5*. With either $q_i(\tau)$ "turned on" and the other $q_i(\tau)$ set to zero ("turned off") [e.g., $q_1(\tau)$ = step function and $q_2(\tau) = 0$, and the converse], the transient part of the solution, $\Delta\Phi(\tau, y)$, satisfies Sturm-Louiville problems on two intervals ($1 \geq y \geq y_0$ and $y_3 \geq y \geq 1$). On each interval, the general solution is a Fourier-Bessel series (7). The eigenvalues are determined by matching the two solutions at $y = 1$. Appropriate Fourier constants [corresponding to $q_i(\tau)$ turned on, for $i = 1, 2$] are determined by satisfying the initial condition, $C_{ss}^0(y)$. We express transient solution in terms of the convolution integrals of the time functions, $q_i(\tau)$, by applying Duhamel's principle (15). Finally, the transient concentration distribution is computed as $C(t, y) = C_{ss}^0(y) + \Phi(\tau, y)\Delta Q^{Max}$. For all three of the NO production scenarios considered here [i.e., step change, pulse change, and continuous (square wave) pulses], *Eqs. A1–A5* can be integrated analytically. However, the final solutions are quite involved and are omitted for brevity.

REFERENCES

1. **Beckman JS and Koppenol WH** Nitric oxide, superoxide, and peroxynitrite: the good, the bad, and ugly. *Am J Physiol Cell Physiol* 271: C1424–C1437, 1996.
2. **Bird RB, Stewart WE, and Lightfoot EN.** *Transport Phenomena*. New York: Wiley, 1960, p. 47, 140–146, 297, 366–370, 503–516, 601–649.
3. **Brandish PE, Buechler W, and Marletta MA.** Regeneration of the ferrous heme of soluble guanylate cyclase from the nitric oxide complex: acceleration by thiols and oxyhemoglobin. *Biochemistry* 37: 16898–16907, 1998.
4. **Butler J.** *The Bronchial Circulation*. New York: Dekker, 1992, p. 53–94.
5. **Butler AR, Megson IL, and Wright PG.** Diffusion of nitric oxide and scavenging by blood in the vasculature. *Biochim Biophys Acta* 1425: 168–176, 1998.
6. **Carroll NG, Cooke C, and James AL.** Bronchial blood vessel dimensions in asthma. *Am J Respir Crit Care Med* 155: 689–695, 1997.
7. **Churchill RV.** *Fourier Series and Boundary Value Problems*. New York: McGraw-Hill, 1941, p. 1–167.
8. **Condorelli P and George SC.** Theoretical gas phase mass transfer coefficients for endogenous gases in the lungs. *Ann Biomed Eng* 27: 326–339, 1999.
9. **Condorelli P and George SC.** A kinetic analysis of soluble guanylate cyclase activation by free nitric oxide. *Biophys J* 80: 2110–2119, 2001.
10. **Denninger JW and Marletta MA.** Guanylate cyclase and the NO/cGMP signaling pathway. *Biochim Biophys Acta* 1411: 334–350, 1999.
11. **Eich RF, Li T, Lemon DD, Doherty DH, Curry SR, Aitken JF, Mathews AJ, Johnson KA, Smith RD, Phillips GN Jr, and Olson JS.** Mechanism of NO-induced oxidation of myoglobin and hemoglobin. *Biochemistry* 35: 6976–6983, 1996.
12. **Gastineau RM, Walsh PJ, and Underwood N.** Thickness of bronchial epithelium with relation to exposure to radon. *Health Phys* 23: 857–860, 1972.
13. **Gaston B.** Nitric oxide and thiol groups. *Biochim Biophys Acta* 1411: 323–333, 1999.
14. **Gaston B, Drazen JM, Loscalzo J, and Stamler JS.** The biology of nitrogen oxide in the airways. *Am J Respir Crit Care Med* 149: 538–551, 1994.
15. **Golomb M and Shanks ME.** *Elements of Ordinary Differential Equations*. New York: McGraw-Hill, 1965, p. 224–242.
16. **Gow AJ, Luchsinger BP, Pawloski JR, Singel DJ, and Stamler JS.** The oxyhemoglobin reaction of nitric oxide. *Proc Natl Acad Sci USA* 96: 9027–9032, 1999.
17. **Herold S, Exner M, and Nauser T.** Kinetic and mechanistic studies of the NO*-mediated oxidation of oxymyoglobin and oxyhemoglobin. *Biochemistry* 40: 3385–3395, 2001.
18. **Huang KT, Han TH, Hyduke DR, Vaughn MW, Van Herle H, Hein TW, Zhang C, Kuo L, and Liao JC.** Modulation of nitric oxide bioavailability by erythrocytes. *Proc Natl Acad Sci USA* 98: 11771–11776, 2001.
19. **Ignarro LJ, Buga GM, Wood KS, Byrns RE, and Chaudhuri G.** Endothelium-derived relaxing factor produced and released from artery and vein is nitric oxide. *Proc Natl Acad Sci USA* 84: 9265–9269, 1987.
21. **Kalsner S.** *Nitric Oxide and Free Radicals in Peripheral Neurotransmission*, Boston: Birkhauser, 2000, p. 57–77, 114–159.
22. **Kharitonov VG, Russwurm M, Magde D, Sharma VS, and Koesling D.** Dissociation of nitric oxide from soluble guanylate cyclase. *Biochem Biophys Res Commun* 239: 284–286, 1997.
23. **Kharitonov VG, Sharma VS, Magde D, and Koesling D.** Kinetics of nitric oxide dissociation from five- and six-coordinate nitrosyl hemes and heme proteins, including soluble guanylate cyclase. *Biochemistry* 36: 6814–6818, 1997.
24. **Lancaster JR Jr.** Simulation of the diffusion and reaction of endogenously produced nitric oxide. *Proc Natl Acad Sci USA* 91: 8137–8141, 1994.
25. **Lancaster JR Jr.** Diffusion of free nitric oxide. *Methods Enzymol* 268: 31–50, 1996.
26. **Lancaster JR Jr.** A tutorial on the diffusibility and reactivity of free nitric oxide. *Nitric Oxide* 1: 18–30, 1997.
27. **Lee JS.** *Frontiers in Biomechanics—Microvascular Hematocrit of the Lung*. New York: Springer, 1986, p. 353–364.
28. **Li X and Wilson JW.** Increased vascularity of the bronchial mucosa in mild asthma. *Am J Respir Crit Care Med* 156: 229–233, 1997.
29. **Liao JC, Hein TW, Vaughn MW, Huang KT, and Kuo L.** Intravascular flow decreases erythrocyte consumption of nitric oxide. *Proc Natl Acad Sci USA* 96: 8757–8761, 1999.
30. **Liu X, Miller MJ, Joshi MS, Sadowska-Krowicka H, Clark DA, and Lancaster JR Jr.** Diffusion-limited reaction of free nitric oxide with erythrocytes. *J Biol Chem* 273: 18709–18713, 1998.
31. **Liu X, Miller MJ, Joshi MS, Thomas DD, and Lancaster JR Jr.** Accelerated reaction of nitric oxide with O_2 within the hydrophobic interior of biological membranes. *Proc Natl Acad Sci USA* 95: 2175–2179, 1998.
32. **Liu X, Samouilov A, Lancaster JR Jr, and Zweier JL.** Nitric oxide uptake by erythrocytes is primarily limited by extracellular diffusion not membrane resistance. *J Biol Chem* 277: 26194–26199, 2002.
33. **Malinski T, Taha Z, Grunfeld S, Patton S, Kapturczak M, and Tomboulian P.** Diffusion of nitric oxide in the aorta wall monitored in situ by porphyrinic microsensors. *Biochem Biophys Res Commun* 193: 1076–1082, 1993.
34. **McKay MD, Beckman RJ, and Conover WJ.** A comparison of three methods for selecting values of input variables in the analysis of output from a computer code. *Technometrics* 21: 239–245, 1979.
35. **Nakata M, Tatsumi T, Tsukiya T, Taenaka Y, Nishimura T, Nishinaka T, Takano H, Masuzawa T, and Ohba K.** Augmentative effect of pulsatility on the wall shear stress in tube flow. *Artif Organs* 23: 727–731, 1999.

35a. **National Research Council (U.S.).** Solubilities of gases in water. In: *International Critical Tables of Numerical Data, Phys-*

ics, Chemistry, and Technology, edited by Washburn E, West CJ, and Dorsey NE. New York: McGraw-Hill, 1928, p. 255–260.
36. **Palmer RM, Ferrige AG, and Moncada S.** Nitric oxide release accounts for the biological activity of endothelium-derived relaxing factor. *Nature* 327: 524–526, 1987.
37. **Qiu Y and Tarbell JM.** Interaction between wall shear stress and circumferential strain affects endothelial cell biochemical production. *J Vasc Res* 37: 147–157, 2000.
38. **Rainville ED and Bedient PE.** *Elementary Differential Equations*. New York: Macmillan, 1974, p. 396–457.
39. **Ravichandran LV, Johns RA, and Rengasamy A.** Direct and reversible inhibition of endothelial nitric oxide synthase by nitric oxide. *Am J Physiol Heart Circ Physiol* 268: H2216–H2223, 1995.
40. **Shin HW and George SC.** Microscopic modeling of nitric oxide and S-nitrosoglutathione kinetics and transport in human airways. *J Appl Physiol* 90: 777–788, 2001.
41. **Silkoff PE.** Noninvasive measurement of airway inflammation using exhaled nitric oxide and induced sputum. Current status and future use. *Clin Chest Med* 21: 345–360, 2000.
42. **Silkoff PE, Robbins RA, Gaston B, Lundberg JO, and Townley RG.** Endogenous nitric oxide in allergic airway disease. *J Allergy Clin Immunol* 105: 438–448, 2000.
43. **Silkoff PE, Sylvester JT, Zamel N, and Permutt S.** Airway nitric oxide diffusion in asthma: role in pulmonary function and bronchial responsiveness. *Am J Respir Crit Care Med* 161: 1218–1228, 2000.
44. **Stone JR and Marletta MA.** Spectral and kinetic studies on the activation of soluble guanylate cyclase by nitric oxide. *Biochemistry* 35: 1093–1099, 1996.
45. **Thomas DD, Liu X, Kantrow SP, and Lancaster JR Jr.** The biological lifetime of nitric oxide: implications for the perivascular dynamics of NO and O_2. *Proc Natl Acad Sci USA* 98: 355–360, 2001.
46. **Tsoukias NM, Tannous Z, Wilson AF, and George SC.** Single-exhalation profiles of NO and CO_2 in humans: effect of dynamically changing flow rate. *J Appl Physiol* 85: 642–652, 1998.
47. **Vaughn MW, Huang KT, Kuo L, and Liao JC.** Erythrocytes possess an intrinsic barrier to nitric oxide consumption. *J Biol Chem* 275: 2342–2348, 2000.
48. **Vaughn MW, Kuo L, and Liao JC.** Estimation of nitric oxide production and reaction rates in tissue by use of a mathematical model. *Am J Physiol Heart Circ Physiol* 274: H2163–H2176, 1998.
49. **Vaughn MW, Kuo L, and Liao JC.** Effective diffusion distance of nitric oxide in the microcirculation. *Am J Physiol Heart Circ Physiol* 274: H1705–H1714, 1998.
50. **Watkins DN, Peroni DJ, Basclain KA, Garlepp MJ, and Thompson PJ.** Expression and activity of nitric oxide synthases in human airway epithelium. *Am J Respir Cell Mol Biol* 16: 629–639, 1997.
51. **Wink DA, Grisham MB, Mitchell JB, and Ford PC.** Direct and indirect effects of nitric oxide in chemical reactions relevant to biology. *Methods Enzymol* 268: 12–31, 1996.
52. **Wink DA and Mitchell JB.** Chemical biology of nitric oxide: insights into regulatory, cytotoxic, and cytoprotective mechanisms of nitric oxide. *Free Radic Biol Med* 25: 434–456, 1998.
53. **Wood J and Garthwaite J.** Models of the diffusional spread of nitric oxide: implications for neural nitric oxide signaling and its pharmacological properties. *Neuropharmacology* 33: 1235–1244, 1994.
54. **Xue C, Botkin SJ, and Johns RA.** Localization of endothelial NOS at the basal microtubule membrane in ciliated epithelium of rat lung. *J Histochem Cytochem* 44: 463–471, 1996.
55. **Zhao Y, Brandish PE, Ballou DP, and Marletta MA.** A molecular basis for nitric oxide sensing by soluble guanylate cyclase. *Proc Natl Acad Sci USA* 96: 14753–14758, 1999.